properties of radioactive materials and methods of measurement

protocol for the laboratory work

Matthias Pospiech, Sha Liu

28th January 2004

Contents

1. theory

1.1. radioactivity

Radioactivity refers to the particles which are emitted from nuclei as a result of nuclear instability. The most common types of radiation are called alpha, beta, and gamma radiation. Radiation from nuclear sources is distributed equally in all directions, obeying the inverse square law. [3]

1.1.1. natural background radiation

We are all exposed to ionizing radiation from natural sources at all times. This radiation is called natural background radiation, and its main sources are the following: [1]

- Radioactive substances in the earth's crust
- Emission of radioactive gas from the earth
- Cosmic rays from outer space which bombard the earth
- Trace amounts of radioactivity in the body

1.1.2. labelling of nuclei

Different nuclei's are labelled as ${}^{A}_{Z}X$. The numbers A and Z denote the corecharge Z (number of protons) and the masscounter A which is the sum of protons and neutrons. A nuclide is thus determined by its numbers A and Z.

1.1.3. alpha decay

Composed of two protons and two neutrons, the alpha particle is a nucleus of the element helium. Because of its very large mass (more than 7000 times the mass of the beta particle) and its charge, it has a very short range. This radiation is characteristic for heavy radioactive elements. [3]

$$ {}^{A}_{Z}X \rightarrow {}^{A-4}_{Z-2}Y + {}^{4}_{2}He $$

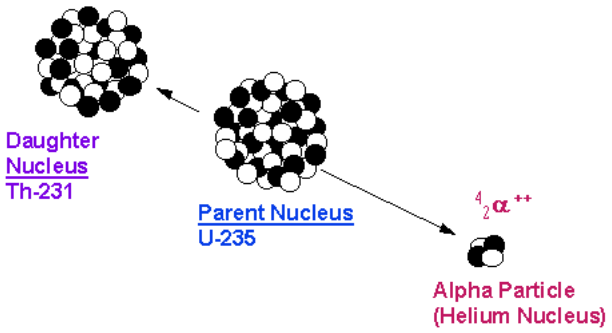

Figure 1: example of alpha radiation process [1]

1.1.4. beta decay

Beta particles are electrons from the nucleus, the term "beta particle" being an historical term used in the early description of radioactivity. The high energy electrons have greater range of penetration than alpha particles, but still much less than gamma rays.

Beta emission is accompanied by the emission of an electron antineutrino which shares the momentum and energy of the decay. The emission of the electron's antiparticle, the positron, is also called beta decay. Beta decay can be seen as the decay of one of the neutrons to a proton via the weak interaction. [3]

$$ {}^{A}_{Z}X \rightarrow {}^{A}_{Z+1}Y + {}^{4}_{2}e^{-} $$

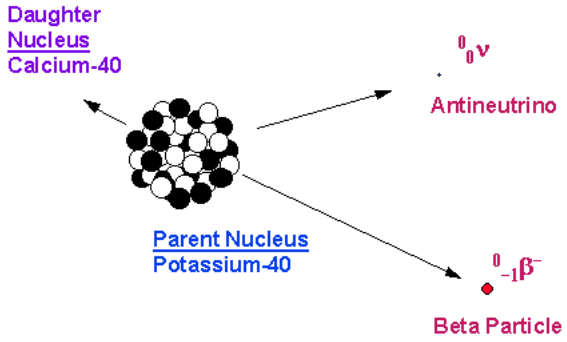

Figure 2: example of beta radiation process [1]

1.1.5. gamma radiation

Gamma radioactivity is composed of electromagnetic rays. It is distinguished from x-rays only by the fact that it comes from the nucleus. Most gamma rays are somewhat higher in energy than x-rays and therefore are very penetrating. It is the most dangerous type of radiation because of its ability to penetrate large thicknesses of material. [3]

In gamma decay, the unstable nucleus shifts from a high energy state to a lower energy state. Since the number of protons in the nucleus has not changed, the decay product is the same element, but in a more stable form. [2]

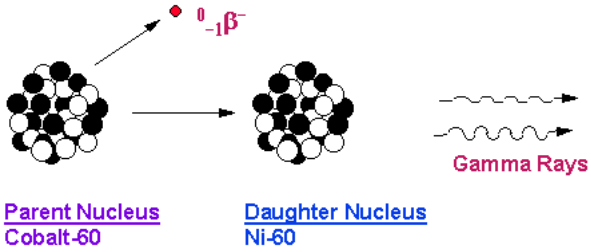

Figure 3: example of gamma radiation process [1]

1.2. properties radioactive radiation

1.2.1. half-life

Radioactive materials decay at exponential rates unique to each radioisotope. Half-life is the time required for a given amount of some radioactive material to be reduced to one-half of its original activity. [1]

The radioactive decay law is

$$N(t) = N_0 e^{-\lambda t}$$

with N, the number of atoms remaining, in terms of the number of atoms N_0 at time 0, and time t. The quantity λ, known as the "radioactive decay rate", depends on the particular radioactive substance. [6]

From this we can deduce the half-life as

$$T_{1/2} = \frac{\ln 2}{\lambda}$$

Using this number we can rewrite the decay law in the form:

$$N(t) = N_0 2^{-\frac{t}{T_{1/2}}}$$

1.2.2. decay rate

The different radioactive cores decay with different speeds, depending on their stability. The decay rate λ (as introduced in 1.2.1) is the number of radiation events per time-unit.

1.2.3. activity

We define the activity as $A(t) = \lambda N(t)$. For the case of exponential decay,

$$A(t) = \lambda N(t) = -\frac{\partial N(t)}{\partial t}$$

Thus activity represents the number of decays per unit time interval. [7]

From the exponential radioactive decay law we obtain

$$A(t) = A_0 e^{-\lambda t}$$

Common units of activity are Becquerel (Bq) and Curie (Ci) though the latter is not a SI unit and should therefore not be used anymore.

- Becquerel (Bq) = 1 dps (disintegration per second)
- Curie (Ci) = 3.7×10^{10} dps

Though the Curie unit is obsolete it is still used by the American Scientific Society. [1]

1.2.4. dose

For the purposes of radiation protection, it is not always useful to describe radioactive material in terms of its activity. It is often preferable to measure radiation by describing the effect of that radiation on the materials through which it passes. The three main quantities which describe radiation field intensity are shown in the following table: [1]

Quantity	Unit	What is Measured
Exposure	Coulombs/kg	amount of charge produced in 1 kg of air by x- or gamma rays
Energy Dose	Gray (Gy)	amount of energy absorbed in 1 gram of matter from radiation
Dose Equivalent	Sievert (Sv)	absorbed dose modified by the ability of the radiation to cause biological damage

Table 1: quantities of doses

1.2.5. Radioactive Decay Paths

Radioactivity involves the emission of particles from the nuclei. In the case of gamma emission, the nucleus remaining will be of the same chemical element, but for alpha, beta, and other radioactive processes, the nucleus will be transmuted into the nucleus of another chemical element. Each decay path will have a characteristic half-life, but some radioisotopes have more than one competing decay path. [3]

1.2.6. Inverse Square Law

In the absence of absorption, the alpha, beta, and gamma rays speed away from the sample uniformly in all directions. From simple geometric arguments follows, that the intensity of radiation follows the inverse square law, i.e., as distance from a point source increases, the intensity decreases proportionally to the square of the change in distance. The intensity of

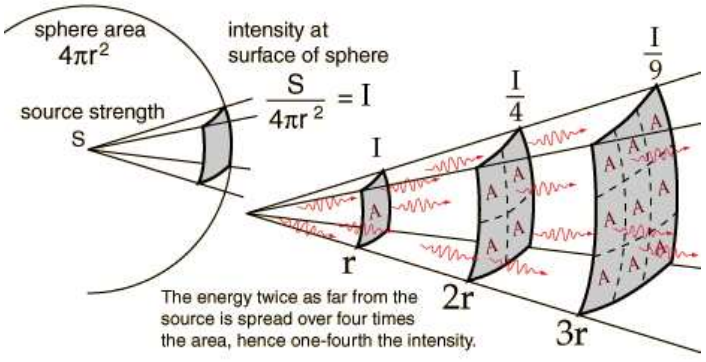

Figure 4: Illustration of the Inverse Square Law [3]

radiation has thus the following dependence

$$I = \frac{A}{r^2}$$

with Activity A and distance from source r. Consequently mean small changes in distance near a source large changes in radiation exposure. [2]

1.3. counting tubes

1.3.1. Geiger-Mueller tube

A Geiger Mueller (GM) tube is a gas-filled radiation detector. It commonly takes the form of a cylindrical outer shell (cathode) and the sealed gas-filled space with a thin central wire (the anode). The fill gas is generally argon at a pressure of less then 0.1 atm plus a small quantity of a quenching vapor (halogen). For detection of low energy beta rays the end window must be sufficient thin. Alpha rays do not pass the windows and can therefore not be detected with such a tube.

The tube and wire are held at a large potential difference (roughly 1000 volts). Normally, the potential difference is not enough for a spark to jump from the wire to the metal wall of the tube. If a gamma ray now interacts with the GM tube (primarily with the wall) it will produce an energetic electron that may pass through the interior of the tube. Ionization along the path of the electrons of the primary electron results in low energy electrons that will be accelerated towards the center wire by the strong electric field. Collisions with the filled gas produce excited states that decay with the emission of a UV photon and electron-ion pairs. The new electrons, plus the original are accelerated to produce a cascade of ionization called "gas multiplication" or a avalanche. Photons emitted can ionize gas liberating additional electrons that produce additional avalanches at sides displaced from the original.

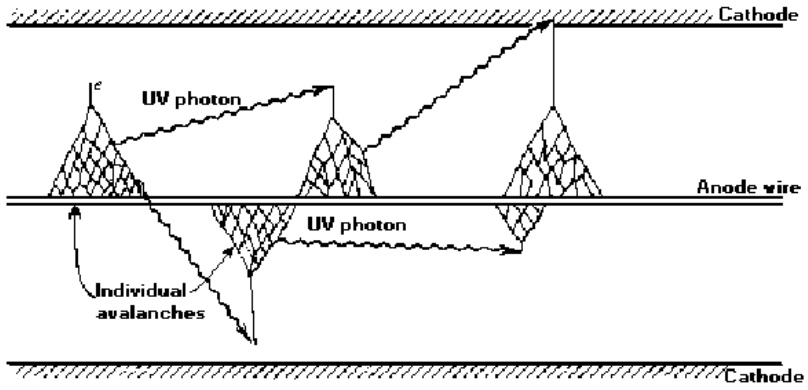

Figure 5: mechanism of avalanches in a Geiger-Mueller discharge [4]

The significant slower massive positive ions could produce new electrons near the cathode starting the process of electron avalanches all over again. This is prevented by using the quenching vapor. In the interaction process with the vapor the energy of the ion is lost in nonradiative energy transfer. [4]

The characteristic (current vs. voltage) of such a tube determined by its threshold voltage and the plateau. From the threshold voltage onwards the counting rate increases proportional with the voltage until the curve becomes flat. This is the plateau region which has two important characteristics: First, the number of electrons produced is independent of applied voltage and second, the number of electrons produced is independent of the number of electrons produced by the initial radiation. The working voltage is therefore chosen in this region. As one increases the voltage furthermore selfdischarges will increase the counting rate dramatically. This leads to a destruction of the tube and must therefore be prevented. [5]

In contrast to other types of proportional counter tubes are pressure and voltage chosen in such a way that the electron avalanches propagate along the wire, with just one initial electron necessary. The Impulses of charge messured are thus independent of type and energy of the incidented radiation particle.

1.3.2. dead time - two source method

The sheath of positive ions close to the anode (wire) reduces the intense electric field sufficiently that approaching electrons do not gain sufficient energy to start new avalanches. The detector is then inoperative (dead) for the time required for the ion sheath to migrate outward far enough for the field gradient to recover above the avalanche threshold. The time required for recovery to value high enough for a new pulse to be generated and counted is called the dead time. [4]

The Geiger Mueller counter becomes dead for typically a few microseconds following the record of an event. The unusual length of the Geiger pulses limits the maximum counting rate and is thus an important disadvantage of the device.

An error in recorded counts arises when the counting has a finite dead-time (τ). A simple correction[1] can be made to the observed count rate (R) provided the dead time is known [5]

$$R' = \frac{R}{1 - R\tau} \qquad R' : \text{real counting rate}$$

If deadtime corrections are not made then underestimation of count rate is possible.

To estimate the dead-time, we use in this experiment the 'two source method'. In this method the sum of two individual countingrates (R_1, R_2) is compared with the countingrate of both samples ($R_{1,2}$) together. Due to the loss of counts is the sum of the individual measurements higher than the one with increased activity.

$$R_1 + R_2 > R_{1,2}$$

Under the estimation that dead-times for the individual measurements are neglectable we obtain the rate displaymath for the 'real' counting values (R_0 : background)

$$R_1' + R_2' = R_{1,2}' + R_0 \tag{1}$$

$$\frac{R_1}{1 - \tau R_1} + \frac{R_2}{1 - \tau R_2} = \frac{R_{1,2}}{1 - \tau R_{1,2}} + R_0 \tag{2}$$

[1] for derivation see reference [5]

With the approximation (for small values τR) $\frac{1}{1-\tau R} \approx 1 + \tau R$ follows

$$\tau = \frac{R_1 + R_2 - R_{1,2} - R_0}{R_{1,2}^2 - R_1^2 - R_2^2}$$

1.4. statistics

The decay of radioactive particle is an incident of pure statistical nature. In a repeated measurement under constant environmental conditions, of impulses over a time interval T one observes the distribution of decays over time. In the case of radiation this is the Poisson distribution [12]:

$$P = \frac{\mu^n}{n!} \mathrm{e}^{-\mu}$$

The mean value is

$$\langle n \rangle = \sum_n nP(n) = \mathrm{e}^{-\mu} \sum_n \frac{n\mu^n}{n!} = \mu \mathrm{e}^{-\mu} \sum_n \frac{\mu^{n-1}}{(n-1)!} = \mu$$

and for the deviation yields with $\langle n^2 \rangle = \mu^2 + \mu$ and $\langle n \rangle^2 = \mu^2$

$$\sigma^2 = \langle n^2 \rangle - \langle n \rangle^2 = \mu$$

Thus the Poisson distribution is only dependent on the parameter μ.

For high numbers n passes the Poisson distribution into the Gaussian Distribution.

In our measurements we deal with two kinds of data:

- In momentarily measurements we deal with a number of ten or more measurements under the same condition. Under the assumption that this data is normal we use the mean number as the resulting value and the deviation as the error.
- In impulse counting measurements we have measured a value of a poisson distributed process. We can not determine (with just one measurement) whether this number corresponds to the mean number ($\mu = N$), but since this is the most probable we simply assume this. The error is then the deviation $\sigma = \sqrt{\mu}$.

1.4.1. error calculations

We have defined the error of the number of counts as $\Delta N = \sigma = \sqrt{N}$.
The error of activity $A = N/t$ is then with tiny error of time measurement Δt:

$$\Delta A = \frac{\partial A}{\partial N} \Delta N + \frac{\partial A}{\partial t} \Delta t \approx \frac{1}{t} \Delta N = \frac{\sqrt{N}}{t} = \sqrt{\frac{A}{t}}$$

2. dose rates

2.1. ambient dose rate, annual dose rate

We have measured the ambient dose rate for 24 hours. There have been no special conditions for this measurement. The result of the measurement is 1.3 μSv per 24 hours.

The mean dose per hour is thus 54 nSV and the annual dose using the mean amount of days per year according to the Julian calendar[2] (a=365.25d) $\approx$ 0.47 mSv.

2.2. dose power of selected natural radioactive materials

The dose rate of the radioactive materials has been taken in distances of 0, 5, and 10 cm from the measurement device. Since the indication of the measuring instrument fluctuates, we have taken series of so called momentarily-measurements and took the statistical results as our data. The background radiation for this place and device was observed as 0.06$\pm$0.02 mSv.

The following table presents the obtained data with corrections for the background. The magnitude of all doses power is in μSv per hour.

material	0 cm	5 cm	10 cm
green glass (uranium doped)	0.06	0.03	0.00
1g mud from Hundsbühl	0.05	0.01	0.00
needle	0.07	0.00	0.01
gas-shell	0.16	0.02	0.02
italian ceramic (uranium)	0.62	0.29	0.14
old clock (^{226}Ra)	3.32	0.51	0.15
CS_{137}	4.49	0.59	0.20

Table 2: radioactive materials

One can see, that the doses in certain distances of most of the sources are not measurable since the radiation is strongly absorbed by the air. The ceramic and old clock nevertheless can penetrate the air by larger distances because they are beta and gamma radiators.

To judge the dose powers we have to compare the values to the maximal daily dose. We therefore calculate the exposure-time necessary to exceed the limit value of 0.2 mGy per hour. The relation between Sievat (Sv) and Gray (Gy) is a quality factor (Q) which takes the possible biological damage into account. We use here Q equal to one.

material	dose / μSv			maximal exposure time / h			annual dose / mSv		
	0 cm	5 cm	10 cm	0 cm	5 cm	10 cm	0 cm	5 cm	10 cm
italian ceramic (uranium)	0.62	0.29	0.14	321	690	1429	5.43	2.54	1.23
old clock (^{226}Ra)	3.32	0.51	0.15	60	392	1333	29.10	4.47	1.31
CS_{137}	4.49	0.59	0.20	45	339	1000	39.36	5.17	1.75

Table 3: maximal exposure times and annual dose of natural radiators

[2] see for example http://www.geocities.com/CapeCanaveral/Lab/7671/julian.htm

Only those materials with comparatively high radiation have been calculated in table 3. The other materials would not give useful results, since the value of maximal exposure time to reach the maximal daily doses is of values of several month.

The ceramic is not very harmful since it takes approximately 2 month to reach the maximal daily dose in 10 cm distance. Whereas the clock must be taken as harmful. The dose at zero distance (which applies when worn) is more than the fourth of the limit value. It is therefore not surprising that the substance used in the clocks for the phosphorescence is nowadays no longer allowed.

2.3. Inverse Square Law

Here we have used a very high active CS-137 source with 16.7 MBq. The dose was measured in distances of 5, 10 and 20 cm. The points are fitted with the expected inverse square function. The diagram shows that the points match the fitted graph very well. The inverse square law can therefore be taken as verified.

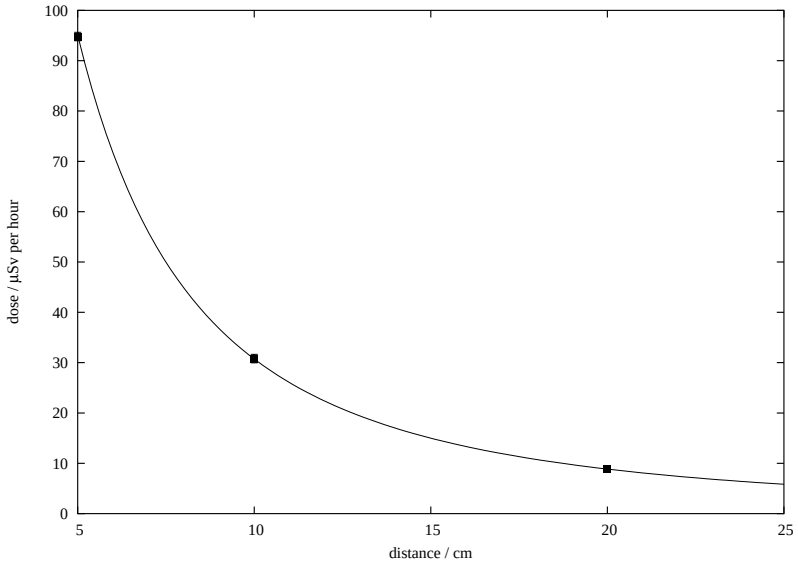

Figure 6: Inverse Square Law

3. Geiger Mueller Counting tube

3.1. properties of Geiger Mueller Counting tube

3.1.1. characteristics

The characteristic was measured in steps of 20 V starting with 680 V up to 1100 V. We did not measure higher voltages to prevent damaging of the tube. The impulses were detected for a time of 1 min. The source of radiation for this measurement was Strontium-90. The characteristic is shown in figure 7. The slope in the plateau is 42.7 impulses per 100 V. The

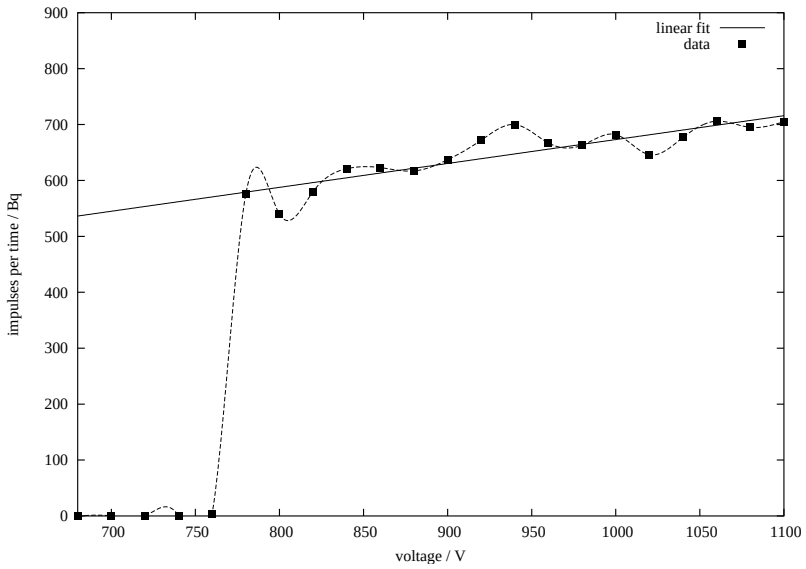

Figure 7: Geiger-Mueller characteristic

starting voltage is around 760 V as it can be seen from the diagram. The operation voltage for the proceeding experiments is set to 900 Volts.

3.1.2. background counting rate

With 900 V a background of 289 impulses was measured in 10 min. This means a background of $R_0 = 0.48$ Bq.

3.1.3. dead-time

We use the following two Sr-90 sources for the 'two-source method': First with 3.65 kBq, second with 3.25 kBq (both measured on the 17.08.00).

The data measured in 60 seconds is $R_1 = 17411/60 \approx 290$ 1/s, $R_2 = 16136/60 \approx 269$ 1/s, $R_{1,2} = 30404/60 \approx 507$ 1/s and $R_0 = 0.48$ 1/s. This yield to a dead time of $\tau = 518$ μs.

3.1.4. statistical purity

The test for statistical purity means to test for a Gaussian distribution (test of normality). Therefore impulses are counted several times with constant conditions of source and Geiger tube. The statistical distribution can thus been recorded. The source is strontium 90.

The Shapiro-Wilk test is a very common test for this problem. We apply a more simple model where the value of the range divided by the standard-deviation is compared to a table of probabilities of error α. In our case this value is with Range $R = 141$ and deviation $\sigma = 31.69$:

$$\frac{R}{\sigma} \approx 4.449$$

According to table 4 in [8] (for a sample of 100) is our distribution normal even with an probability of error of 10%. We can therefore assert our distribution to be normal.

Graphically this is more obvious if one plots the sum of probabilities with a special probability scale . In this diagram a normal distribution appears as a straight line. This is shown in figure 9.

α	range
0.0 %	1,99 - 14.07
0.5 %	4,03 - 6.53
1.0 %	4,10 - 6.36
2.5 %	4,21 - 6.11
5.0 %	4,31 - 5.90
10.0 %	4,45 - 5.68

Table 4: ranges for different probabilities of error

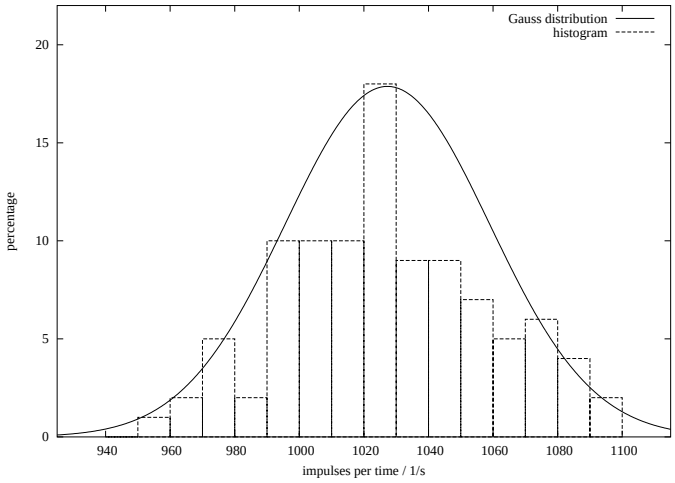

Figure 8: statistical distribution of counts

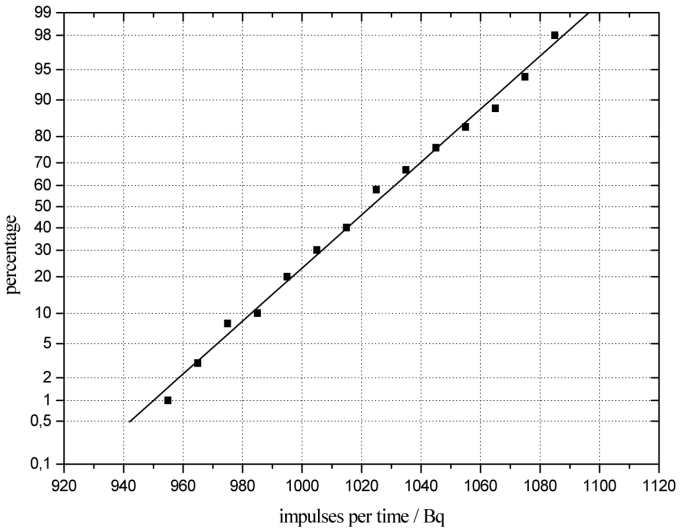

Figure 9: sum distribution in probability scale diagram

3.1.5. counting efficiency

The purpose of this experiment is to observe the efficiency of the GM-tube for different types of radiation. The radiation is selected by choice of six different radiators. The gamma radiation is measured with a plate of aluminium over the source to shield the beta radiation. The efficiency is different depending on the distance from the tube. This is taken into account by two measurements, one in ≈ 1.5 cm and another in ≈ 5 cm distance between source and GM-tube. The results are shown in table 5.

The alpha radiation is very strong absorbed in air. It is therefore not surprising that the efficiency decreases largely. The beta radiation can penetrate larger distances of air. The higher value of Sr-90 is due to the higher energy of the beta particles compared to the other radiators. The efficiency of the gamma radiators is low because the measurement relies on a secondary process.

			counts		activity / Bq		efficiency in %	
source	type	activity / Bq	1.5 cm	5 cm	1.5 cm	5 cm	1.5 cm	5 cm
Pu-238	α	816	2078	43	34.63	0.72	4.24	0.09
Sr-90	β	3113	17327	3258	288.78	54.30	9.28	1.74
Co-60	β	457	943	150	15.72	2.50	3.44	0.55
Tl-204	β	5413	1457	258	24.28	4.30	0.45	0.08
Co-60	γ	26151	2173	705	36.22	11.75	0.14	0.04
Cs-137	γ	34549	651	220	10.85	3.67	0.03	0.01

Table 5: efficiency of GM tube for different types of radiation

3.1.6. efficiency of the sheath

Since gamma radiation can only be measured through electrons produced in the sheath of the tube, this has an important effect on the efficiency of the detection of gamma-rays. This means that too thin walls produce too less electrons, whereas too thick walls absorb the electrons too much. Here we test two different materials (gold, lead).

The test was carried out using a beta and gamma (Cs-137) and a beta radiator (Na-22) and the two materials for the sheathing. The counting rate was taken for one minute each. the efficiency was calculated using the current activities for both sources: Cs-137: 33.846 kBq, Na-22: 9.294 kBq.

	impulses			activity		efficiency	
sheath	background	Cs	Na	Cs	Na	Cs	Na
none	46	566	577	8.67	8.85	0.036	0.095
gold	40	671	597	10.52	9.28	0.031	0.100
lead	28	544	587	8.60	9.32	0.025	0.100

Table 6: efficiency of the sheath

We observe, as it should be expected a decrease of the gamma background radiation with gold and lead. The activity of Cs-137 increases with gold, but is lower with lead. This is because of the high attenuation of gamma rays in lead. The Na-22 contrary shows a low increase of activity from gold to lead.

3.2. radiation properties

3.2.1. absorption of beta radiation

In this absorption measurements as well as in the next attenuation measurement for gamma radiation we measure the time until we reach 500 counts. The idea behind this is to have a low error of measurements, which might be significantly higher if we had measured the counts per time, since the measured activity can become quite low in this measurements.

Here we want to observe the properties absorption of beta radiation in different materials. We use Sr-90 as source (recent activity: 3.23 kBq).

From the resulting plots (respectively the fits) we can the determine the half-thickness. This means the thickness of the material necessary to reduce the intensity of the original radiation to one-half of its initial value. It is determined by $d_{1/2} = \ln 2 \cdot t_{\text{fit}}$

From the graph we can expect an exponential decay. We apply therefore a fitfunction

$$f(x) = A\mathrm{e}^{-x/t}$$

The resulting plots are shown in figures 10 and 11. We obtain the values $t_{\text{Al}} = 0.82\,\text{mm}$ and $t_{\text{PET}} = 2.00\,\text{mm}$. This yields to values of $d_{1/2}(\text{Al}) = 0.57\,\text{mm}$ and $d_{1/2}(\text{PET}) = 1.38\,\text{mm}$ for the half-thicknesses of the materials.

Based on the density of the materials we can recalculate the half thickness into the density thickness. The density of aluminium is $2.70\ \text{g/cm}^3$ [10] so that we get $0.057\,\text{cm} \cdot 2.70\,\text{g/cm}^3 =$

$0.1539\,\mathrm{g/cm^2}$. From this value one can recalculate the maximal energy of the beta radiation. The supplied diagram is used for this determination. The formula of Flammersfeld can unfortunately not be applied because we cannot determine the maximal range of the radiation. The result is a maximal energy of about 2.5 MeV. The correct value in balance with its daughter nuclide is 2.282 MeV [13]. This value is matched quite well considering the high error in reading off the diagram.

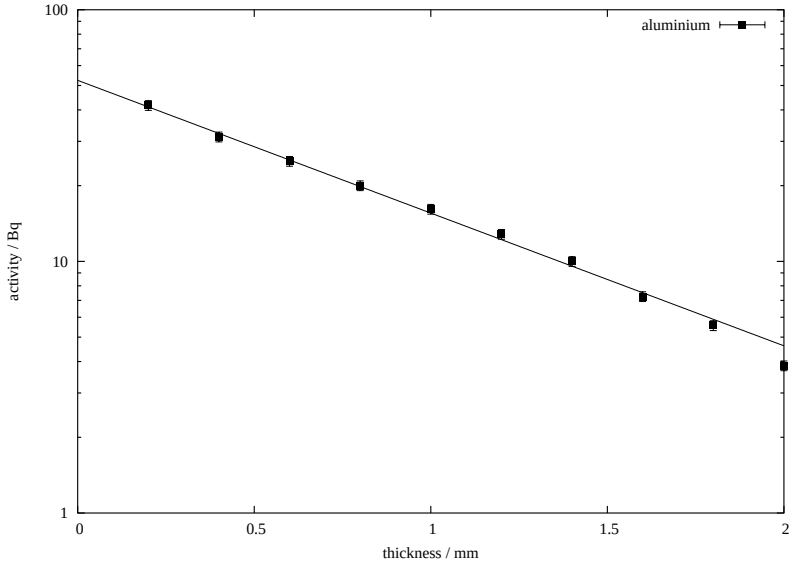

Figure 10: absorption of beta radiation in aluminium

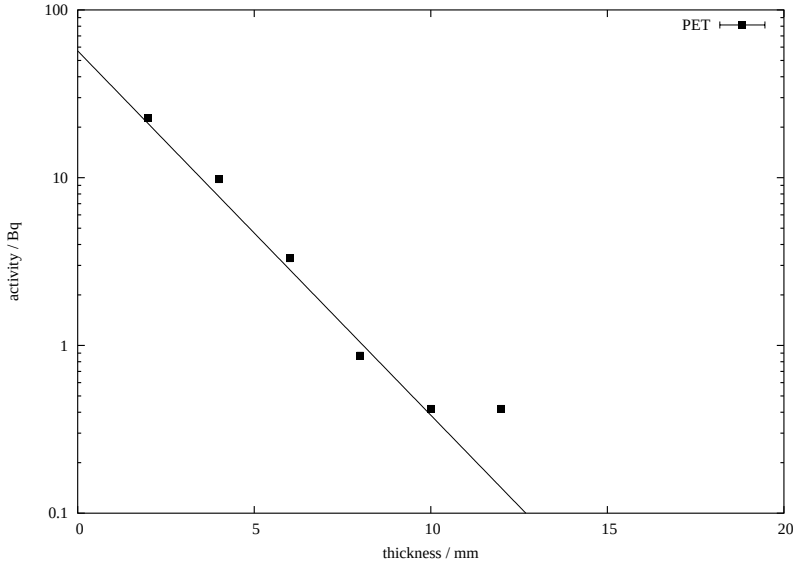

Figure 11: absorption of beta radiation in polyethylene (PET)

3.2.2. attenuation of gamma radiation

The same experiment as before is now carried out with gamma radiators. The main difference is that the radiation cannot be absorbed completely but will only be attenuated. We use lead and iron as absorbing materials and record the activity for two different sources (Co-60, Cs-137). The density of these materials are iron: 7.86 g/cm^3, lead: 11.34 g/cm^3 [10]. The results are summarized in table 7. The calculations thereby are done as shown in the previous section. The according plots are in figures 12 and 12.

source	absorber	ϱ in g/cm^3	t_{fit}/mm	$d_{1/2}$/mm	$\varrho \cdot d_{1/2}$ in g/cm^2	E_{max} in MeV
Co-60	iron (Fe)	7.86	34.60	23.98	18.85	≈ 2
Co-60	lead (Pb)	11.34	23.44	16.24	18.43	≈ 2
Cs-137	iron (Fe)	7.86	25.28	17.52	13.77	≈ 1.4
Cs-137	lead (Pb)	11.34	12.28	8.51	9.65	≈ 0.9

Table 7: gamma half-thicknesses of different materials

The reference values for the maximum energies are: Co-60: 2.506 MeV and Cs-137: 0.66 MeV [13]. Unfortunately our values do not match these reference values very well.

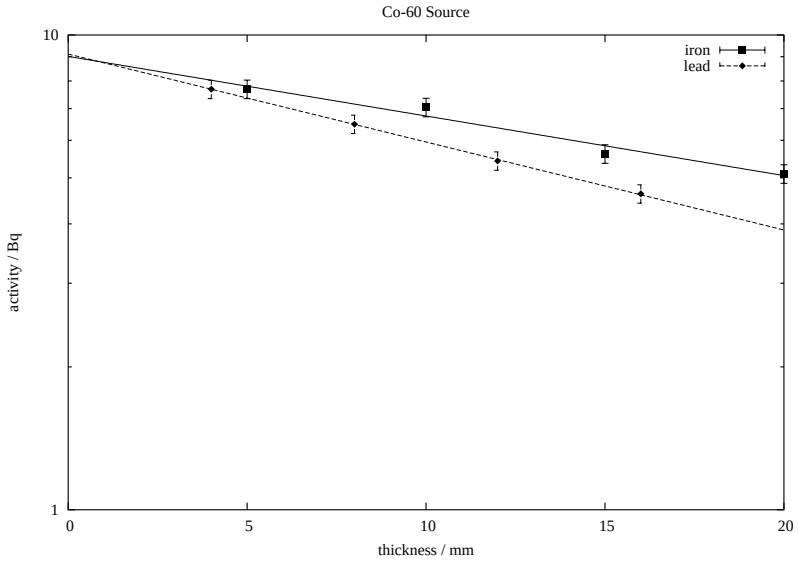

Figure 12: gamma attenuation of Co-60 gamma radiation

3.2.3. backreflection of beta radiation

As we have seen in the consideration of the inverse square law is only a small proportion of the radiation, in dependence of the solid angle and the distance, incidented on the measurement device. In case radiation was incidented after reflection from the opposite side the activity would increase. Here we want to determine the properties of backreflected radiation and its dependence on the reflection material.

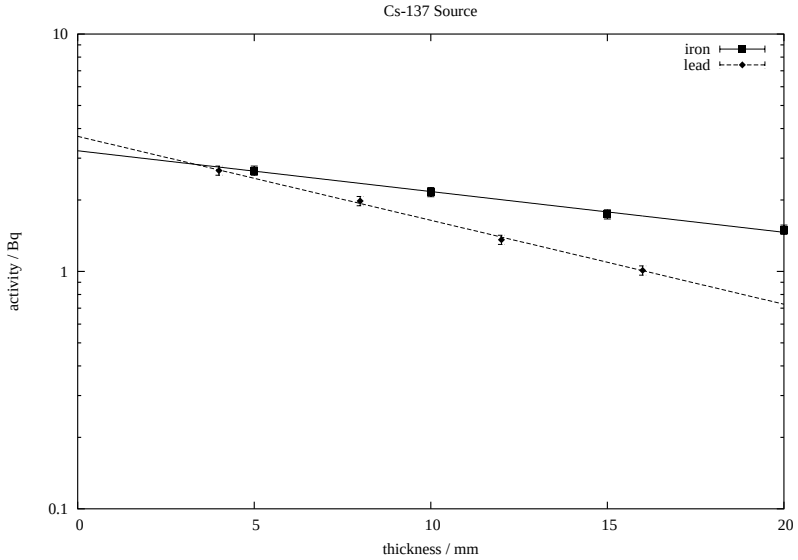

Figure 13: gamma attenuation of Cs-137 gamma radiation

The reason for the backscattering in matter is the deflection of electrons due to coulomb interaction with the core. This only changes the forward direction of a beta particle by a few degrees. Backscattering is thus a effect of multiple scattering.

Due to this properties we should expect a dependence on the thickness of the material, because the interaction range is higher and the atomic number because higher corecharge mean higher interaction. Upon reaching the maximal backreflection the backreflection goes into saturation. This means that matter above the saturation thickness does not contribute to the backreflection anymore.

Both experiments are carried out using a source placed inside a weak absorbing thin foil. The activity was measurement for 30 seconds. Very thin plates of gold are used to increase the thickness of the material. To prevent damage of the source the plates are placed on top of each other with a tweezer. The background recorded for 10 minutes is 0.52 Bq.

As expected we can see in figure 14 an activity which goes into saturation as the thickness increases. From the shape of the graph the saturation thickness can not be clearly defined. We estimation it to be of a value of 0.05 mm.

thickness / mm	counts	activity / Bq
0.00	512	16.54
0.02	666	21.68
0.04	709	23.11
0.06	688	22.41
0.08	711	23.18
0.10	732	23.88
0.12	722	23.54

Table 8: backscattering in gold in dependence on the thickness

material	Z	counts	activity / Bq	backreflection rate
none	0	482	15.54	1.00
acrylglass	2	539	17.44	1.12
glass	12	582	18.88	1.21
aluminium (Al)	13	582	18.88	1.21
iron (Fe)	26	618	20.08	1.29
nickel (Ni)	28	605	19.64	1.26
copper (Cu)	29	661	21.51	1.38
silver (Ag)	47	708	23.08	1.48
indium (In)	49	667	21.71	1.40
tungsten (W)	74	713	23.24	1.50
gold (Au)	79	767	25.04	1.61
lead (Pb)	82	706	23.01	1.48

Table 9: backscattering in dependence on the atomic number

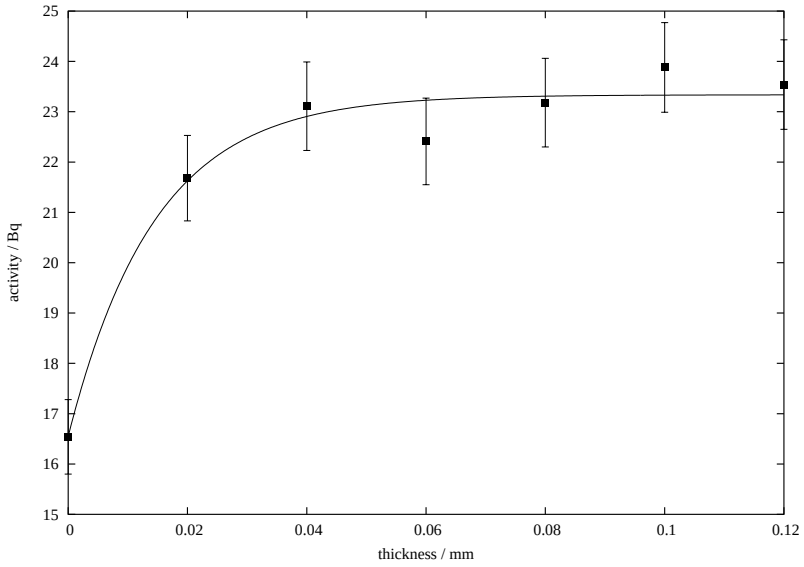

Figure 14: backreflection in dependence of the thickness

The background and measurement method are maintained for the second experiment. Here different materials, which are available in their saturation thickness, are used for the backreflection measurement. The graph in figure 15 shows the backreflection rate. Its curve shows the expected increase with rising corecharge Z.

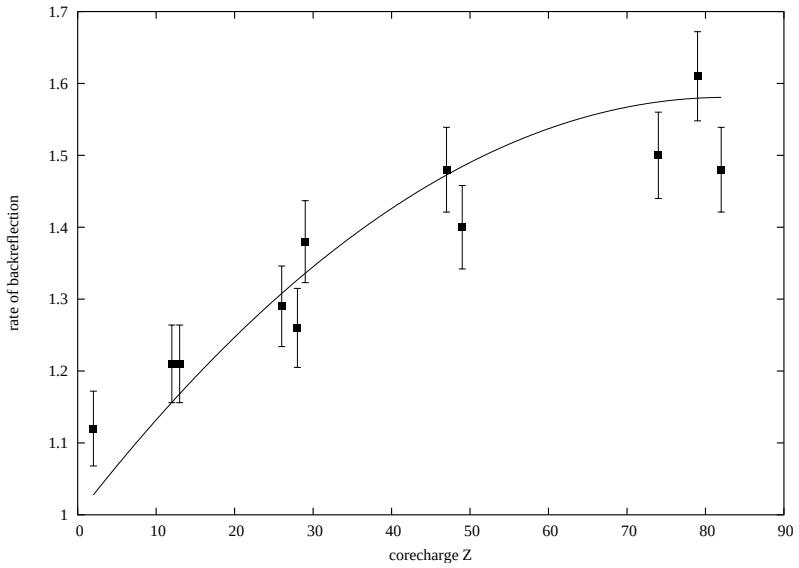

Figure 15: backreflection in dependence of the corecharge of the material

3.3. additional methods

3.3.1. isotope generator

The purpose of this experiment is to determine the halftime of Pa-234 (protactinium). This element has a very short halftime[3] of 1.175 min. This very short lifetime and the fact that it is highly toxic make this element very difficult to handle. To make the radiation of this element nevertheless available one can use a isotope generator.

The main idea of an isotope generator is that the deserved nuclide is available through the decay path of a different nuclide (U-238), but kept inside a container in an aqueous solution. The container contains in addition to the water solution a second organic liquid (keton) which is lighter than water and does not dissolve in it. The protactinium though dissolves much better in this liquid than in water. Thereby one can isolate the Pa-234 locally by shaking the container, so that keton and Pa-234 admix and accumulate at the top of the container. The parent (uranium) and daughter (protactinium) nuclide which are in equilibrium are thereby separated so that the Pa-234 can be measured independently.

First we measure the background as 3.2 Bq with the isotope generator unshaken (in equilibrium), since this additional radiation will appear in the background of the actual measurement. This value has not been subtracted from the following data since some points decreases below this background. The measurement was stopped as soon as we could be sure that we will not observe a decrease any more.

From the fit we calculate a halftime of $T_{1/2} = \ln 2 \cdot 146.75 \text{ s} = 101.72 \text{ s} = 1.69 \text{ min}$. This is significantly higher than the correct value of 1.175 min. The initial increase is due to the fact that the keton has to accumulate on top of the water which takes some time.

[3] value taken from the datasheet of the isotope generator

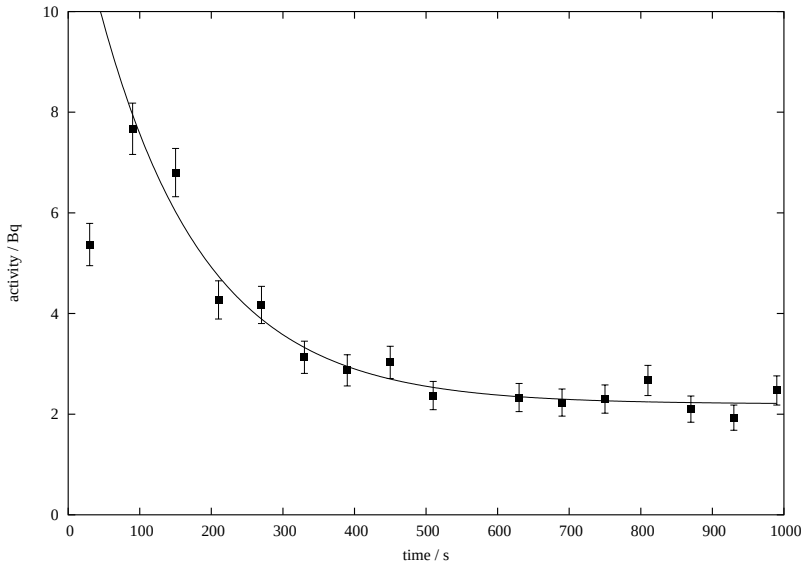

Figure 16: decay of Pa-234 (isotope generator)

time /s	impulses	activity / Bq
30	161	5.37
90	230	7.67
150	204	6.80
210	128	4.27
270	125	4.17
330	94	3.13
390	86	2.87
450	91	3.03
510	71	2.37
630	70	2.33
690	67	2.23
750	69	2.30
810	80	2.67
870	63	2.10
930	58	1.93
990	74	2.47

Table 10: activity of isotope generator

3.3.2. radiometric determination of potassium

Potassium contains isotopes which are radioactive. This can be used to determine the concentration of a KaCl solution. Since the amount of potassium is proportional to the concentration and thus its radiation proportional to the concentration this can be used to determine the concentration.

First we have to take a calibration curve. Thereby we determine the relation between

activity and concentration. This was done using six different concentrations. For each we have recorded more than ten activities as momentarily measurements. This have quite high fluctuations which result in the high error of the activity. The data and the calibration line is shown in figure 17. The calibration line is $f(x) = 1.4907 + 0.0505 \cdot x$.

The unknown concentrations have the activities: $A_1 = 1.76 \pm 0.21$ and $A_2 = 2.11 \pm 0.34$. This values yield to concentrations of $C_1 = 5.29 \pm 4.16\,\%$ and $C_2 = 12.16 \pm 6.76\,\%$. This values show that the measurement is not very accurate. The high errors result from the high standard deviation of the activities recorded.

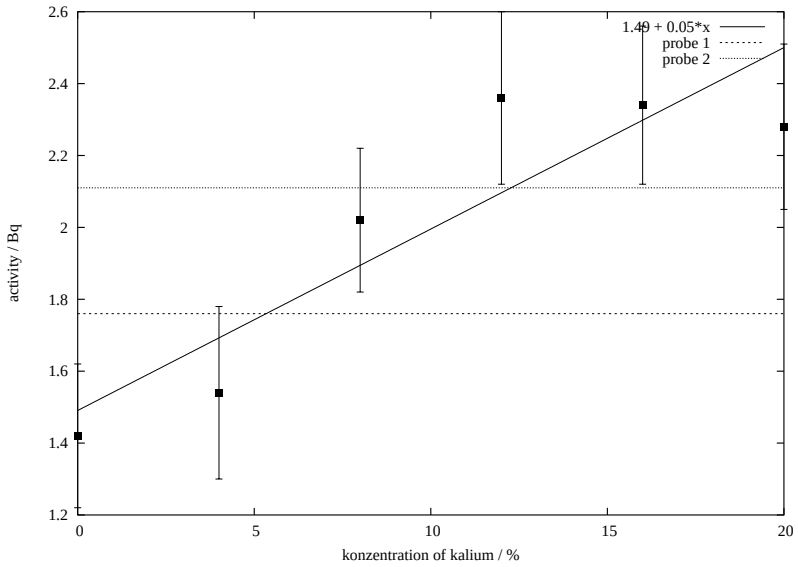

Figure 17: concentration vs. activity of potassium

concentration	activity / Bq	deviation / Bq
0	1.42	0.20
4	1.54	0.24
8	2.02	0.20
12	2.36	0.24
16	2.34	0.22
20	2.28	0.23

Table 11: determination of potassium

4. Neutron sources

In our experiment, we use Americium-241/beryllium as the radioisotropic neutron sources. Neutron techniques are of wide applications, because neutrons are highly penetrating in high atomic number materials. When the material is of bulk nature or is contained within metallic or other dense materials, one can use neutron detector techniques.

There are two kinds of neutron detecting techniques: first, passive neutron techniques which rely upon the detection of natural neutron emissions (neutrons originating from the material itself) without relying on any external excitation of the sample; second, active neutron techniques which may be employed when the isotopes in the sample do not emit sufficient spontaneous neutrons to permit precise measurements to be made within a realistic time period, or when a direct measurement of a fissile isotope is required.

4.1. ambient dose rate

During the experiment we use a BF3 gas filled proportional counter to measure the working environment. Near the neutron source, the radiation intensity is 7.0 mSv/h, in the work place, the radiation intensity is 1.7 μSv/h.

4.2. Attenuation of neutron radiation

After measuring the ambient dose rate, thick board is added one by one on top of the neutron source. The number of neutrons per minute is recorded as the thickness of the board grows. Four different materials are used: wax, iron, aluminium, glass.

The duration measure time is 1min, and working voltage at 2100V.

thickness /piece	activity / $\frac{\text{impulse}}{\text{min}}$
0	4044
1	2715
2	1980
3	1575
4	1253
5	1011
6	872
7	740
8	617
9	558
10	546

Table 12: attenuation of neutrons by Wax(20mm)

thickness / piece	activity / $\frac{\text{impulse}}{\text{min}}$
0	4044
1	3245
2	2601
3	2185
4	1907
5	1577
6	1330
7	1118
8	1041
9	965
10	832

Table 13: attenuation of neutrons by iron (20mm)

thickness / piece	activity / $\frac{\text{impulse}}{\text{min}}$
0	4044
1	3707
2	3229
3	2837
4	2529
5	2232
6	2004
7	1860
8	1683
9	1570
10	1376

Table 14: attenuation of neutrons by aluminium (20mm)

thickness / piece	activity / $\frac{\text{impulse}}{\text{min}}$
0	4044
1	3276
2	2819
3	2426
4	1972
5	1769
6	1483
7	1390
8	1218
9	1048
10	980

Table 15: attenuation of neutrons by glass(20mm)

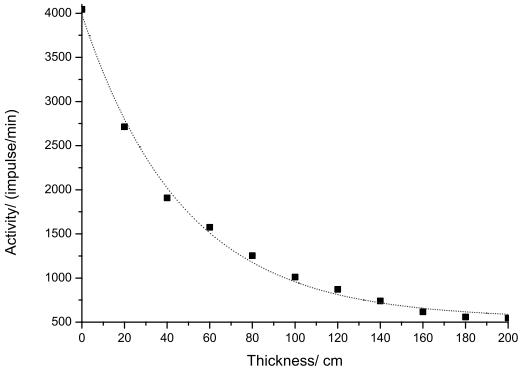

Figure 18: attenuation of neutrons by Wax

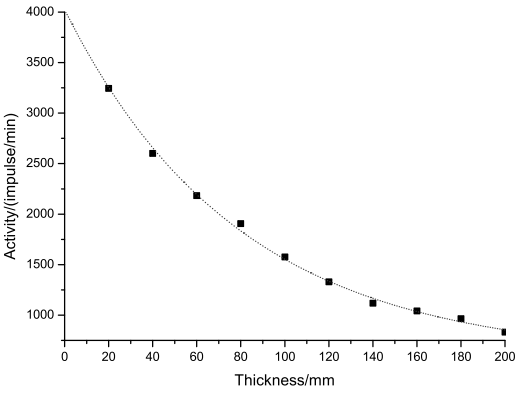

Figure 19: attenuation of neutrons by iron

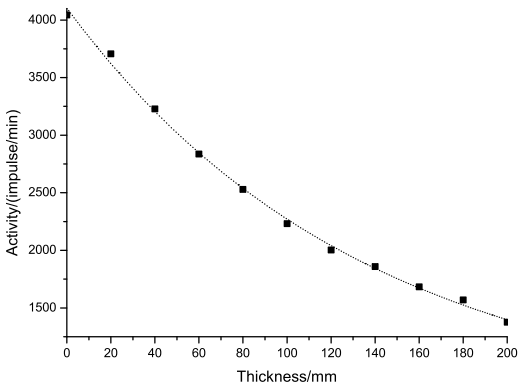

Figure 20: attenuation of neutrons by aluminium

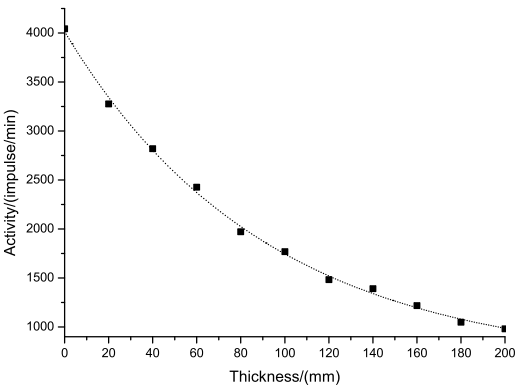

Figure 21: attenuation of neutrons by glass

Generally, the absorption effect of material depends on the function of exponential decay, so exponential decay function is used here to fit the data of attenuation.

$$Y = Ae^{-\frac{x}{\lambda}} + B$$

- Y=number of particles detected
- A=Amplitude of decay
- λ=penetrating depth
- B=background

Material	λ (penetrating depth /mm)
wax	47.4
Fe	79.2
Al	134.9
glass	91.3

Table 16: attenuation of different materials

From the table 16, we can see clearly that the absorption of wax is strongest compared with other materials. To explain the phenomenon we have to consider the structure of atom. In the atom, only the nuclear core has effect on the incoming neutron, electrons are too light to have any effect. And the neutron only can be caught by nuclear core with almost the same mass, if the mass difference is too large, the neutron will be reflected, just as the case in classical elastic collision. For wax, it is a H-atom-rich material, so the absorption effect comes mainly from the H atoms.

4.3. Flux density of thermal neutrons

The majority of the neutrons normally present in neutron beams from nuclear research reactors are thermal neutrons. Cold neutrons can be defined as neutrons with energies below 10mev, an energy which corresponds to velocity and wavelength values of 1400 m/s and 30 nm, respectively. Cold neutrons have longer wavelength and lower kinetic energies on the average than thermal neutrons. Neutron detection equipment for use in industrial facilities is generally based upon 3He gas-filled proportional counters, they have superseded the BF3 counters mainly due to health and safety considerations. For the neutron source of Americium-241/Beryllium, there are thermal neutrons and non-thermal neutrons. Since Cadmium absorbs thermal neutrons, the difference between the shielded and unshielded measurement gives out the thermal neutron flux density.

Here wax plate of thickness 40mm is added one by one on the neutron source. The measure time is 1 min, working voltage 1260V.

In graph 22, the top line stands for the detected radiation without shielding, middle line stands for the detected radiation with Cadmium shielding, the bottom line stands for the difference between the above two lines, that is the amount of thermal neutrons.

thickness/piece	activity / $\frac{\text{impulse}}{\text{min}}$		
	without Ca shielding	Ca shielding	thermal neutron
0	24847	3465	21382
1	78994	7527	71467
2	81031	5143	75888
3	57658	3469	54189
4	42194	2809	39385
5	33572	2557	31015
6	30171	2166	28005
7	27539	2233	25306

Table 17: Flux density of thermal neutrons

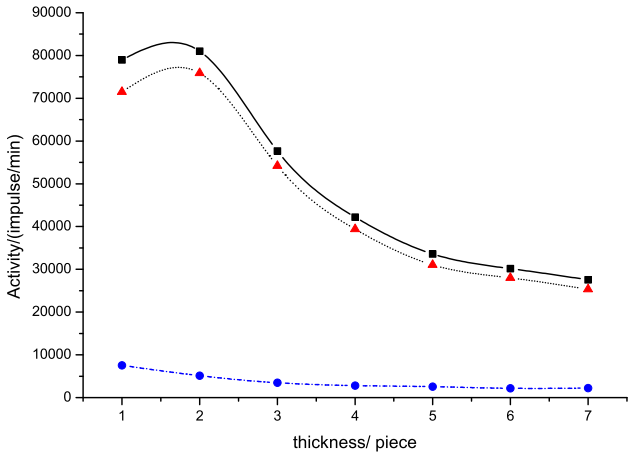

Figure 22: neutron-flux-density

The counter is put at one side above the source, so now mainly reflected neutrons are detected. The radioactive intensity depends on two effect, reflection and absorption, that is why the activity first grows, reaches the maximum at about 60mm, and then decays.

4.4. Prompt gamma radiation

Gamma rays are emitted by a target material which is irradiated with neutrons. New nuclei are formed by capturing the neutrons, and have an excitation energy equal to the binding energy of the added neutron. The excitation energy is released by emission of gamma rays. When the counter is shielded, also prompt gamma rays can be emitted by shielding materials. So with Cadmium shielding, the recorded activity of prompt gamma radiation is stronger than unshielded. As can be seen in graph 23. In graph 23, the upper line stands for the Cadmium shielding prompt gamma radiation, the middle line stands for without shielding prompt gamma radiation, the bottom is the difference between them.

Concentrations of various elements in a sample can be determined from the measured emission rates of characteristic prompt gamma rays produced by neutron capture. γ-ray emission intensity is depended on the intensity of neutrons. As mentioned in 4.3, the activity of neutron depends on reflection and absorption, so is the gamma ray radiation intensity.

Wax plates each of thickness 40mm are used to add on neutron source. Geiger-Müller counter is used here. The measure time is 1 min, working voltage 1920V.

Piece	activity / $\frac{\text{impulse}}{\text{min}}$		
	unshielded	shielded	difference
0	3258	4337	1079
1	3927	6833	2906
2	4293	7037	2744
3	4338	6103	1765
4	4108	5506	1398
5	3691	4713	1022
6	3513	4467	954
7	3337	4103	766

Table 18: prompt gamma radiation

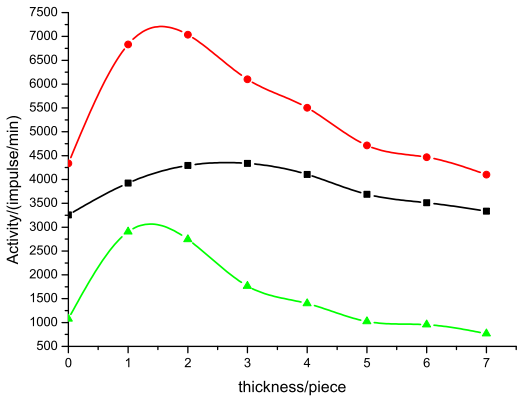

Figure 23: prompt gamma radiation

4.5. Activation and measurement of short half-lives

As mentioned in the beginning of 4, in neutron detecting techniques, there are passive and active neutron techniques. Here the isotopes in the sample do not emit sufficient spontaneous neutrons to permit precise measurements within a realistic time period. So samples are first activated in a capacitor. The capacitor is a mental buck with 6 holes around it, marked as NO1 to NO6. The silver sample is put in NO1 position for 10 Min, and sample rhodium is put in position 6 for 15 Min. Then the samples are put under automatically working Geiger-Müller counter with 10 seconds as the interval. The background is measured before, and is subtracted from the detected activity.

As mentioned in 1.2.1, Radioactive materials decay at exponential rates unique to each radioisotope. Here each sample is composed of two kinds of source, one has a long half-life time $(Ag^{1}08, Rh^{1}04m)$, the other has a short half-life time$(Ag^{1}10, Rh^{1}04)$. So in the beginning of the whole decay process, radiation of short half-life time source is dominant; near the end, the radiation of long half-life time source is major part. For the two different stages, linear fit is used independently to find the λ.

The radioactive decay law is

$$N(t) = N_0 e^{-\lambda t} \Rightarrow lnN = lnN_0 - \lambda t$$

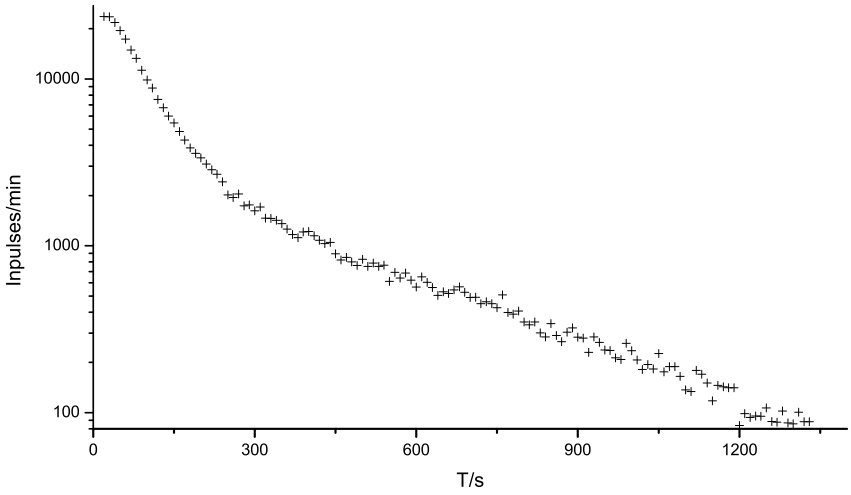

Figure 24: Half-life-time of Rh(whole range)

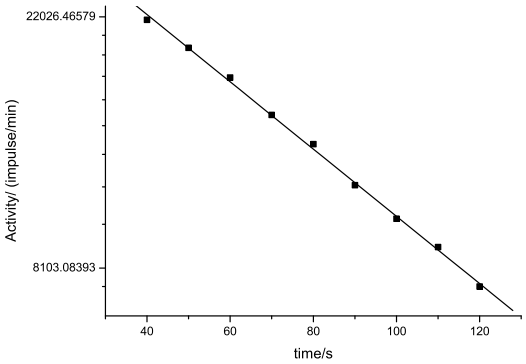

Figure 25: short half-life-time Rh-104

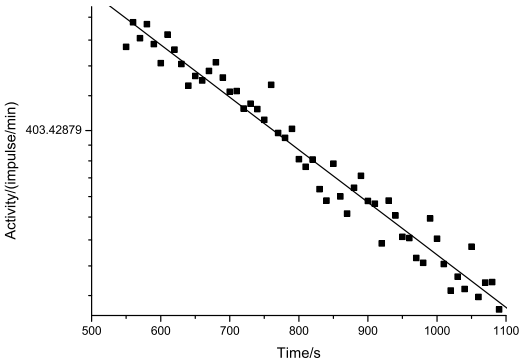

Figure 26: long half-life-time Rh-104m

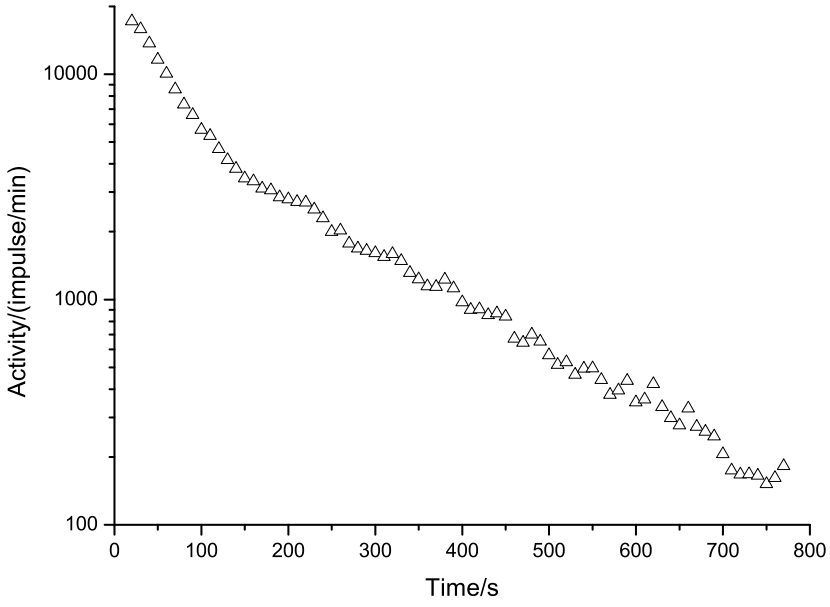

Figure 27: Half-life-time of Ag(whole range)

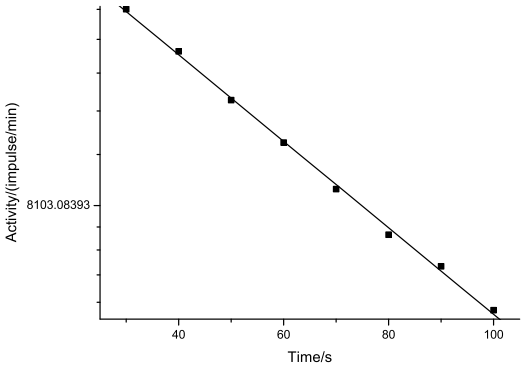

Figure 28: short half-life-time Ag-110

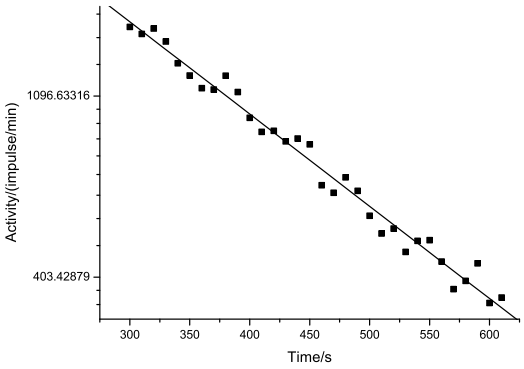

Figure 29: long half-life-time Ag-108

Half-life is the time required for a given amount of some radioactive material to be reduced to one-half of its original activity. From this we can deduce the half-life as

$$T_{1/2} = \frac{\ln 2}{\lambda}$$

source	fit range/s	λ	$T_{1/2}/s$
Rb-104	40-230	0.0134	52
Rb-104m	550-1100	0.0226	264
Ag-110	30-100	0.0148	47
Ag-108	300-610	0.0051	136

Table 19: Half life time of Silver and Rhodium

4.6. Law of activation and saturation

After external excitation of the sample, it can be activated, and neutron flux density can be measured. Six probes each with 2g NH_4VO_3 are put around the neutron source, and measured separately after various time age. The background is measured by the detector and is subtracted automatically. From the graph, one can see the sample is saturated after approximately 15Mins.

time/min	activity / $\frac{\text{impulse}}{\text{min}}$
2	11749.67
4	18889.67
6	24375.67
10	29178.67
15	32696.66
25	32718.67

Table 20: law of activation and saturation activity

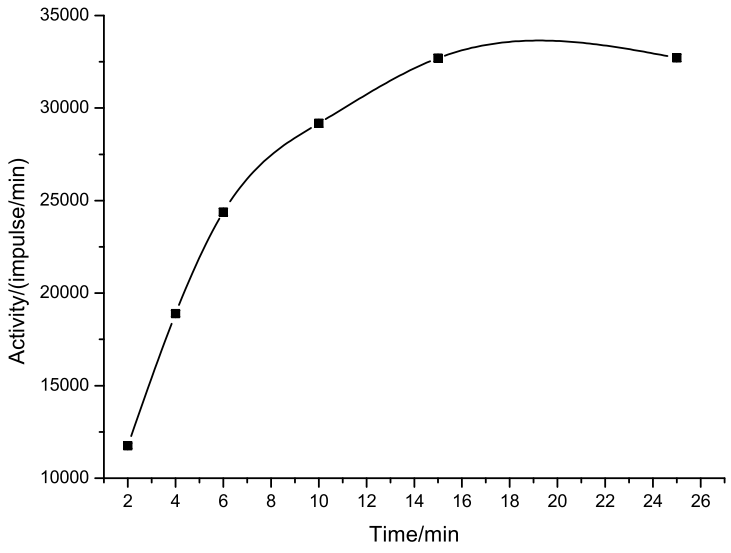

Figure 30: activation and saturation curve

5. proportional counter

We use Pu346 to get the α radiation characteristic curve, and Tl204 to get the β radiation characteristic curve. The data is used to determine the starting and operation voltage, usually operation voltage is chosen in the plateaus region, but the voltage should not be too large in case the damage of equipment. In the proportional counting tube, α and β radiation are in the different voltage range. The background radiation at 1080V is 118/10Min's, that is 0.2Bq. The measure time is 1 min.

Voltage/V	activity / $\frac{\text{impulse}}{\text{min}}$
780	3
840	55
900	757
960	4840
1020	8065
1080	10330
1140	11982
1200	12986
1260	13651
1320	14133
1380	14382
1440	14592
1500	15075

Table 21: alpha radiation

Voltage/V	activity / $\frac{\text{impulse}}{\text{min}}$
1680	25
1740	185
1800	435
1860	868
1920	1427
1980	2326
2040	3496
2100	5306
2160	6966
2220	8541
2280	9428
2340	10279
2400	10873
2460	11358
2520	11538
2580	11785

Table 22: beta radiation

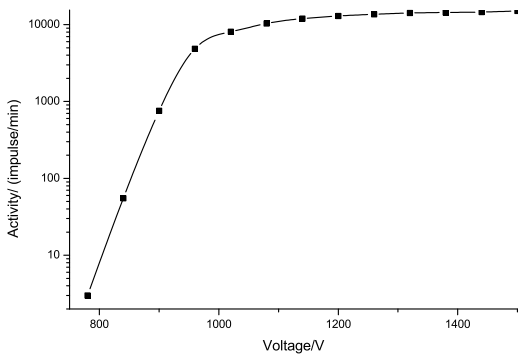

Figure 31: alpha radiation characteristic curve

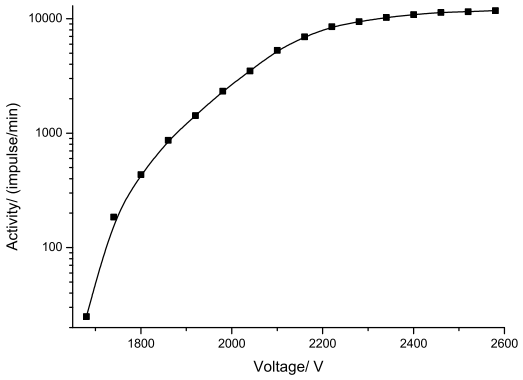

Figure 32: beta radiation characteristic curve

At the different Alpha and Beta working voltage, we measure different samples and calculate the activity and counting efficiency.

radiation	starting voltage/V	operation voltage/V
α	800	1200
β	1620	2400

Table 23: Starting and operation voltage

As mentioned in the theory part 1.2.1, we know how to calculate the activity of sources with units given in Bq and Ci, for natural uranium the calculation is different.

$$A = 1.32 \times 10^6 \frac{m}{MT_{1/2}}$$

- A =activity
- m=mass of the radioactive material
- M =mole mass
- $T_{1/2}$ =half life time

Source	Percentage/ %	m/ mg	$T_{1/2}$ =/ y	A/Bq
U-238	99.2745	0.16	4.468×10^9	1.97
U-235	0.72	0.16	7.038×10^8	0.0019
U-234	0.0055	0.16	2.455×10^5	2.022
total activity 4.0 Bq				

Table 24: calculation of natural uranium's activity

Source	Activity	half-life/y	A-now/Bq	A- measured/Bq	Efficiency %
Pu-238 α	901 Bq	87.7	874.6	216.13	24.7
Tl-204 β	1140 Bq	3.78	572.0	181.22	31.7
Sr-90 β	3250 Bq	28.79	3018.5	2306.5	76.4
C-14 β	9.7 nCi	5730	358.0	92.73	25.9
Am-241 α	16.4 nCi	432.2	588.6	159.75	27.1
Am-241 β	16.4 nCi	432.2	588.6	227.9	38.7
Co-60 β	755 Bq	5.27	460.4	121.58	26.4
natural uranium α	0.16mg	4.468×10^9	4.0	0.47	11.7
natural uranium β	0.16mg	4.468×10^9	4.0	2.18	54.6

Table 25: counting efficiency

6. Contamination monitor

6.1. plate sources

Large contaminated plates of different kinds of materials are detected to determine the counting efficiency, and we try to find the relationship between the counting efficiency and nuclear energy. Here we use Xenon-counter(density $5\frac{mg}{cm^2}$), Butan-counter(density $0.4\frac{mg}{cm^2}$). Plates are set in distance of 0cm, 5cm, 10cm, each time 10 measurements are recorded, and then mean value is calculated.

The counting efficiency of plate is defined as the measured activity over activity per area, each plate is $988cm^2$.

$$S = \frac{I}{A/F}$$

- S=counting efficiency
- I=measured activity
- A=source activity
- F=area of the plate

Source	Activity	half-life/y	measured date	A-now/KBq
Am-241	2.64 kBq	432.2	02/11/1987	2.57
C-14	101 nCi	5730	17/08/1978	3.73
Cl-36	3.73 kBq	3.1×10^5	01/11/1987	3.73
Cs-137	2.98 kBq	30.2	10/11/1987	2.06
Sr-90	9.9 nCi	28.79	15/08/1978	1.99
U-238	105 mg	4.468×10^9	08/08/1978	2.68

Table 26: Information about the source

source	I / $impulse \cdot min^{-1}$		
	0cm	5cm	10cm
Am-241	82	28	24
C-14	44	20	18
Cl-36	193	105	99
Cs-137	121	107	102
U-238	121	91	68

Table 27: Measured activity by Xenon-counter

source	counting efficiency $/cm^2$		
	0cm	5cm	10cm
Am-241	31.40	10.72	9.19
C-14	11.65	5.30	4.77
Cl-36	51.12	27.81	26.22
Cs-137	48.44	36.93	27.82
Sr-90	60.38	53.39	50.90
Naturuan	44.61	33.55	25.07

Table 28: Efficiency by Xenon-counter

source	I / $impulse \cdot min^{-1}$		
	0cm	5cm	10cm
Am-241 β	4163	256	213
Am-241 α	188		
C-14 β	4175	234	304
Cl-36 β	8672	5600	3450
Cs-137 β	5191	2920	192
Sr-90 β	9620	6500	4120
Naturuan β	5881	2740	1910
Naturan α	11		

Table 29: Measured activity by Butan-counter

source	counting efficiency $/cm^2$		
	0cm	5cm	10cm
Am-241 β	26.57	1.63	1.36
Am-241 α	1.2		
C-14 β	18.43	1.03	1.34
Cl-36 β	38.29	24.72	15.23
Cs-137 β	41.50	23.24	1.53
Sr-90 β	80.00	54.06	34.26
Natururan β	36.14	16.84	11.74
Natururan α	0.7		

Table 30: Efficiency by Butan-counter

From above one can see that: as the distance between contaminated plate and detector increases, the counting efficiency decrease. As the detector goes higher and higher, it counts only part of the source activity.

Source	Energy of ray/ Kev
Am-241	59
C-14	158
Cl36	710
Cs-137	520
Sr-90	2270
Naturuan	2300

Table 31: rays' energy of different sources

6.2. point sources

Now come to point sample, they are put at different positions to see the position's effect in detecting.

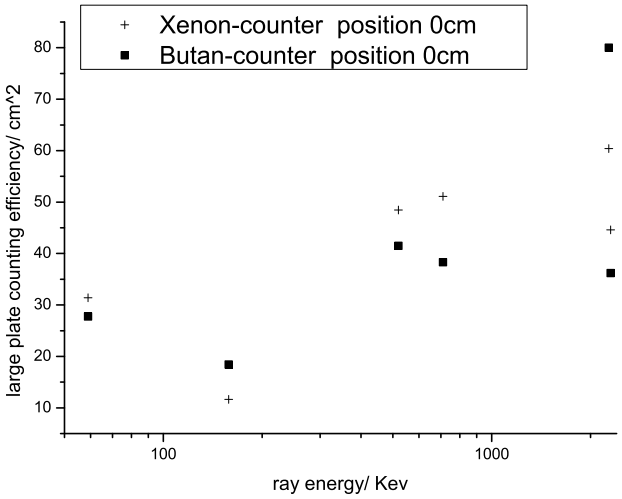

Figure 33: relationship between large plate counting efficiency and the source ray energy

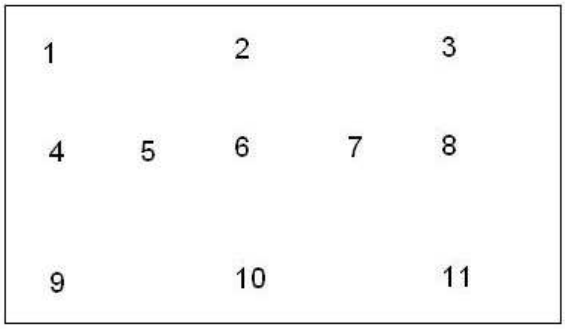

Figure 34: Positions of point source

place	1	2	3	4	5	6	7	8	9	10	11
activity/Bq	87	106	94	102	110	109	110	103	95	108	101

Table 32: position effect on detecting

The phenomenon can be described in the following way: in No2,5,6,7,10, the detected activity is higher, on the edge, the detected activity is lower, in the corner, it is obvious low. Because the detecting center is in 6, we take it as center point drawing circles with different radians, as the length of radian increases, it is more far away from detector, so detected activity is low.

6.3. measurement of contamination

The activity of a Uran contaminated metal plate is to be measured. First a contamination monitor is used to determine the contaminated region. And then, this region is wiped by a filter paper. By measure the activity of the filter paper, the activity of plate is determined.

At first the background is measured, 4 impulse/10min, that is A_b=0.0067 Bq.

Second, the counter is calibrated by a well-known material Naturuan.

Activity of naturuan is 0.16mg, that is A=4.0Bq, the measured activity is A_m=282 imp/10min, that is 0.47Bq, and the calibration coefficient k is

$$k = \frac{A}{A_m - A_b} = \frac{4.0}{0.47 - 0.0067} = 8.63$$

The activity of the filter paper is measured 118 imp/min, that is 1.97Bq, and then caculated back to get the real activity.

$$A = k \cdot (A_m - A_b) = 8.63 \times (1.97 - 0.0067)Bq = 16.9Bq$$

Now the activity of contaminated plate A^* is to be estimated. Assume the measured activity is only 10% of the whole activity, called p. The plate is F=100 cm^2.

$$A^* = \frac{A}{p \cdot F} = \frac{16.9}{0.1 \times 100} = 1.7Bq/cm^2$$

For Uran, in normal circumstance, the maximum radiation intensity is $1\frac{Bq}{cm^2}$, in dangerous area the intensity is 10 $\frac{Bq}{cm^2}$, and in controlled area is 100 $\frac{Bq}{cm^2}$, the lab environment is still safe

A. Appendix

A.1. radioactive decay paths

The data was taken from the 'Korea Atomic Energy Research Institute Table of Nuclides' [9] and the 'LBNL Isotopes Project' at LUNDS Universitet [11]. The decay path figures were taken from the website of 'ChemGlobe' [10].

$$^{14}C \xrightarrow[5730y]{\beta^-} {}^{14}N$$

$$^{22}Na \xrightarrow[2.6019y]{\beta^+} {}^{22}Ne$$

$$^{36}Cl \begin{cases} \xrightarrow[301000y]{\beta^-} {}^{36}Ar\,(98.10\%) \\ \xrightarrow[301000y]{\beta^+} {}^{36}S\,(1.90\%) \end{cases}$$

$$^{60}Co^* \xrightarrow[10.467min]{\gamma} {}^{60}Co \xrightarrow[5271y]{\beta^-} {}^{60}Ni$$

$$^{90}Sr \xrightarrow[28.79y]{\beta^-} {}^{90}Y \xrightarrow[64.00h,3.19h]{\beta^-,\gamma} {}^{90}Zr$$

$$^{137}Cs \xrightarrow[30.07y]{\beta^-} {}^{137}Ba^* \xrightarrow[2.552min]{\gamma} {}^{137}Ba$$

$$^{204}Tl \begin{cases} \xrightarrow[3.78y]{\beta^-} {}^{204}Pb\,(97.10\%) \xrightarrow[1.4\cdot10^{17}y]{\alpha} {}^{200}Hg \\ \xrightarrow[3.78y]{\beta^+} {}^{204}Hg\,(2.90\%) \end{cases}$$

$$^{238}Pu \xrightarrow[87.7y]{\alpha} {}^{234}U \xrightarrow[245500y]{\alpha} {}^{230}Th \longrightarrow \ldots$$

$$^{241}Am \xrightarrow[432.2y]{\alpha} {}^{237}Np \xrightarrow[2144000y]{\alpha} {}^{233}Pa \longrightarrow \ldots$$

element	name
C	carbon
N	nitrogen
Na	sodium
Ne	neon
Cl	clorine
Ar	argon
S	sulfer
Co	cobalt
Ni	nickel
Sr	strontium
Y	yttrium
Zr	zirconium
Cs	cesium
Ba	barium
Tl	thallium
Pb	lead
Hg	mercury
Pu	plutonium
U	uranium
Th	thorium
Am	americanium
Np	neptunium
Pa	protactinium

Table 33: Table of used Elements

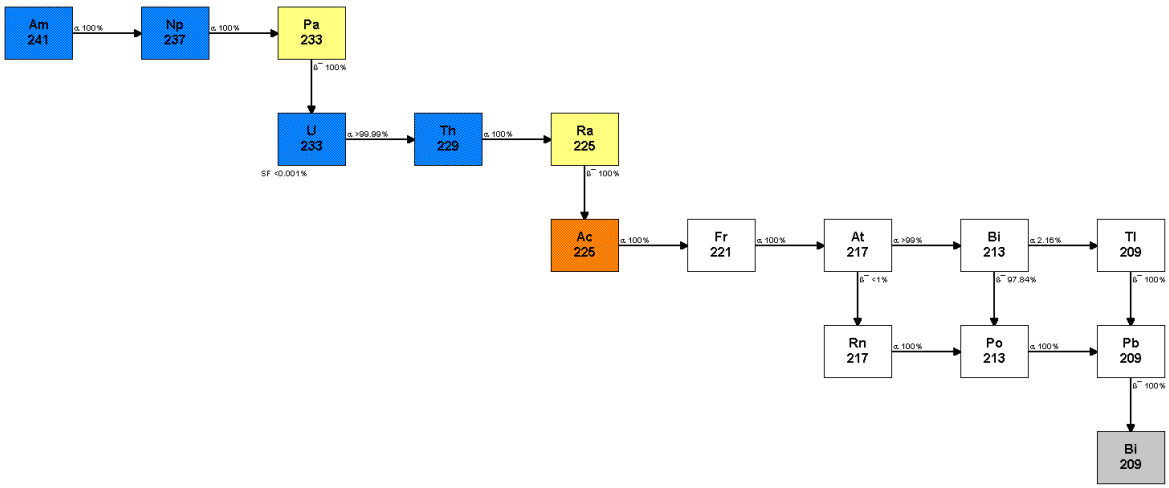

Figure 35: decay path of Am-241 [10]

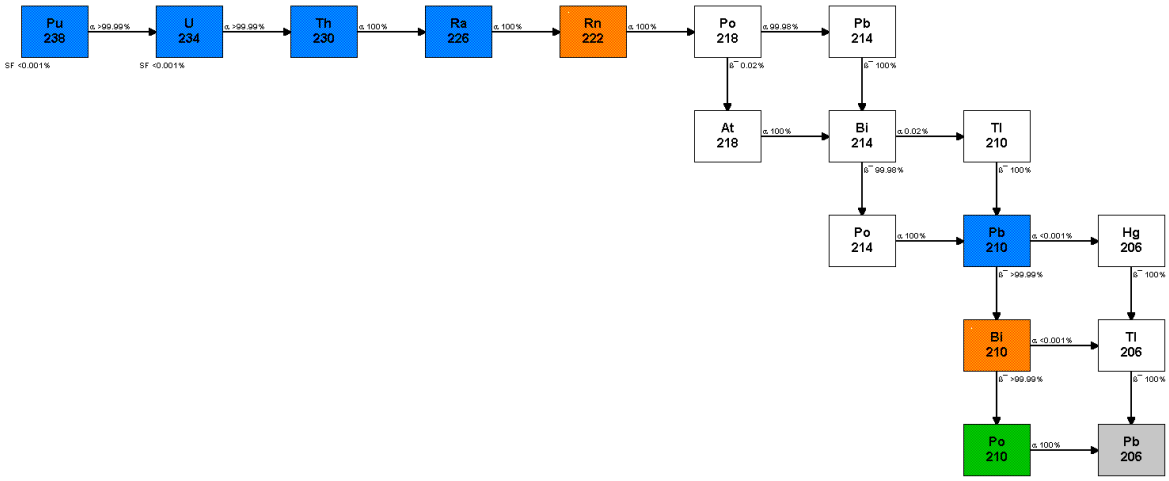

Figure 36: decay path of Pu-238 [10]

A.2. activity of radioactive materials

The date of measurement was set to the 2nd of December 2003. The value Δt represents the time difference in years between this date and the reference date. The recent activity is calculated according to the decay-law:

$$A_{\mathrm{now}} = A_0 \; 2^{-(\Delta t / T_{1/2})} \tag{3}$$

source	ID	date	activity	type	half-live	Δt / years	recent activity /Bq
Na-22	FY849	01.05.98	41.2 kBq	β^+	2.6019y	5.59	9294
Co-60	HL430	01.09.00	40.1 kBq	γ, β	5.271y	3.25	26151
Co-60	GW347	10.11.99	779 Bq	γ, β	5.271y	4.06	457
Sr-90	HL432	17.08.00	3.37 kBq	β	28.79y	3.29	3113
Sr-90	unknown	17.08.00	3.65 kBq	β	28.79y	3.29	3372
Sr-90	unknown	17.08.00	3.25 kBq	β	28.79y	3.29	3002
Sr-90	HL435	17.08.00	3.50 kBq	β	28.79y	3.29	3233
Cs-137	FV658	01.05.98	39.3 kBq	γ, β	30.07y	5.59	34549
Cs-137	FV659	01.05.98	38.5 kBq	γ, β	30.07y	5.59	33846
Tl-204	GW335	10.11.99	1.14 kBq	β	3.78y	4.06	5413
Pu-238	GW333	10.11.99	843 Bq	α	87.7y	4.06	816

Table 34: recent activity of radioactive materials

List of Tables

List of Figures

References

[1] Princeton University http://web.princeton.edu/sites/ehs/ssradtraining/workingsafely/workingsafely.htm

[2] Southern Methodist University http://www.physics.smu.edu/~scalise/emmanual/radioactivity/lab.html

[3] Georgia State University: Hyperphysics http://hyperphysics.phy-astr.gsu.edu/hbase/forces/isq.html

[4] The Pennsylvania State University (Niel Brandt) http://www.astro.psu.edu/users/niel/astro485/derivations/geiger1.pdf

[5] Integrated Publishing http://www.tpub.com/content/doe/h1013v2/css/h1013v2_67.htm

[5] Fachhochschule Karlsruhe (Prof. Dr. Meier-Hirmer) www.home.fh-karlsruhe.de/~mero0001/master/deadtime.pdf

[6] *Radioactive decay and exponential laws*, Ian Garbett http://plus.maths.org/issue14/features/garbett/

[7] University of Cape Town http://www.phy.uct.ac.za/courses/phy300w/np/ch1/node30.html

[8] Statistik Tutorial http://barolo.ipc.uni-tuebingen.de/pharma/3/3.5/

[9] Korea Atomic Energy Research Institute Table of Nuclides http://atom.kaeri.re.kr/

[10] ChemGlobe http://www.vcs.ethz.ch/chemglobe/ptoe/index.html

[11] LBNL Isotopes Project - LUNDS Universitet http://ie.lbl.gov/toi/

[12] http://www.rz.uni-frankfurt.de/piweb/lowtemp/Bruls_Prakt/html_auf_Euroline2/0101_MT5.html

[13] The main book from the experiment - title unknown